Geomorphology 123 (2010) 364–369

Contents lists available at ScienceDirect

Geomorphology

journal homepage: www.elsevier.com/locate/geomorph

Determining lateral migration rates of meandering rivers using fallout radionuclides

E. Black [a], C.E. Renshaw [a,*], F.J. Magilligan [b], J.M. Kaste [c], W.B. Dade [a], J.D. Landis [a]

[a] Department of Earth Sciences, Dartmouth College, Hanover, NH 03755, USA
[b] Department of Geography, Dartmouth College, Hanover, NH 03755, USA
[c] Department of Geology, College of William and Mary, Williamsburg, VA 23187, USA

ARTICLE INFO

Article history:
Received 8 February 2010
Received in revised form 30 July 2010
Accepted 3 August 2010
Available online 18 August 2010

Keywords:
Meanders
Lateral migration
Radionuclides
Floodplain
Sedimentation

ABSTRACT

We explore the novel technique of using short-lived fallout radionuclides to date fluvial surfaces with the goal of determining lateral migration rates. Specifically, we use the fallout radionuclide ^{210}Pb (half-life $t_{1/2}$ ~22.3 years) to determine the lateral migration rates of meandering reaches on the Winooski River, VT, the upper Connecticut River, NH, and the Genesee River, NY. We find that, particularly near the channel, $^{210}Pb_{ex}$ inventories are affected by the initial $^{210}Pb_{ex}$ inventories of freshly deposited sediment (inheritance). Inheritance differs at each site, with lower inheritance occurring at sites with larger upstream drainage areas. After accounting for inheritance, $^{210}Pb_{ex}$ inventories in surface sediments along a transect orthogonal to the channel yield migration rates of 0.7, 3.1, and 4.7 m/y for the Winooski, Connecticut, and Genesee Rivers, respectively. These rates agree well with values derived independently from historical aerial photography. Variations in $^{210}Pb_{ex}$ inventories along the transects also provide details of the channel migration histories not evident from the limited available aerial photographs, including evidence for both nearly constant linear and episodic channel migrations. Results suggest the broad applicability and added value of our approach for quantifying decadal-scale variations in fluvial surface ages.

1. Introduction

River channel lateral migration — often a dominant control on the spatial pattern and rate of sediment sequestration and delivery (Aalto et al., 2008) — has critical implications for geochemical cycling (Billen et al., 1991), contaminant transport (Marcus et al., 2001; Papacostas et al., 2008), and riparian ecosystem impacts from natural and anthropogenic alterations to river flows (Svendsen et al., 2009). Determining migration rates using direct methods (such as erosion pins, historical surveys, and aerial photography) is resource intensive and requires an extensive, high resolution historical database that is often unavailable or impractical to create (Nanson and Hickin, 1983; Lawler, 1993; Hooke, 2008). Here we investigate the applicability of short-lived fallout radionuclides to reconstruct floodplain histories and quantify channel geometry change. More specifically, we compare channel migration rates determined using the short-lived fallout radionuclide ^{210}Pb to those determined using historical aerial photography. We chose ^{210}Pb because its half-life (22.3 years) is similar to the timescale over which aerial photography is available and, more importantly, to the timescale over which active meandering channels migrate.

Short-lived fallout radionuclides have been increasingly used to quantify a broad suite of geomorphic processes, including sediment transport in arid plains (Kaste et al., 2006), hillslope erosion and sedimentation (Wallbrink and Murray, 1996), and sediment generation (Clapp et al., 2000). More recently, short-lived radionuclides have been used to investigate sediment transport dynamics in both unregulated and regulated fluvial systems (Salant et al., 2007; Aalto et al., 2008; Svendsen et al., 2009). If this technique can be adapted to date floodplain ages, it may prove to be a broadly applicable methodology for quantifying decadal-scale sediment exchanges between rivers and their floodplains because it requires no historical surveying, photography, or assumptions regarding the time required for vegetation to colonize newly created floodplains. It thus has fewer limitations than existing techniques for quantifying historical channel geometry changes.

2. Approach

While the dominance of lateral accretion is not universal (Nanson, 1986), we restrict our attention to migrating river bends where lateral accretion is the dominant mechanism driving changes in channel geometry. Limited vertical accretion may occur, particularly proximal to the channel (Aalto et al., 2008), but our focus is on sites where channel lateral migration rates are orders of magnitude greater than typical vertical accretion rates. Thus we expect that variations in floodplain surface ages along transects orthogonal to reaches to closely correspond to the rate of channel migration. Sensitivity analyses indicate that for the sites considered here having lateral migration

* Corresponding author. Tel.: +1 603-646-3365; fax: +1-603-646-3922.
E-mail address: Carl.E.Renshaw@Dartmouth.edu (C.E. Renshaw).

0169-555X/$ – see front matter © 2010 Elsevier B.V. All rights reserved.
doi:10.1016/j.geomorph.2010.08.004

rates of ~1 m/y or more, our estimated lateral migration rates are largely insensitive to vertical accretion for vertical accretion rates <~1 cm/y (more below).

After a laterally accreting floodplain is created along a river bend, its upper surface is exposed to the atmosphere and begins to accumulate atmospheric fallout. If the atmospheric deposition rate is constant, then the age of the surface is proportional to its total inventory of radionuclides. Of particular interest here is the fallout radionuclide ^{210}Pb, one of several short-lived intermediates in the ^{238}U decay series that can be written in abridged form as

$$^{238}\text{U}\rightarrow{}^{226}\text{Ra}\rightarrow{}^{222}\text{Rn}\rightarrow{}^{210}\text{Pb}\rightarrow{}^{206}\text{Pb}$$

^{238}U has a long half-life ($t_{1/2}=4.5$ billion years), and as a consequence, its decay acts as a pseudocontinuous source of ^{226}Ra. Thus, in a closed system all the daughters of ^{238}U decay will be in secular equilibrium, defined as each daughter element having the same activity, $n\lambda$, where n is the number of atoms present and λ the decay constant.

In near-surface sediments and soils, which are open systems, gaseous ^{222}Rn ($t_{1/2}=3.8$ days) partially diffuses to the atmosphere. There it subsequently decays to ^{210}Pb and then returns to the surface as atmospheric fallout, primarily by wet deposition (Appleby and Oldfield, 1992). While there is significant variation in ^{210}Pb deposition rates over short timescales, mean annual deposition at a given location appears to be relatively constant from year to year (Appleby, 2008). Lead is highly surface reactive and, once deposited, quickly sorbs onto sediment particles (Kaste et al., 2003). Thus, in near-surface soils and sediments an "excess" of ^{210}Pb (^{210}Pb$_{ex}$) exists relative to the levels supported by the direct decay of ^{222}Rn.

As the inventory of ^{210}Pb$_{ex}$ increases, the rate of decay of the inventory also increases and approaches the rate of deposition. As equilibrium between atmospheric deposition and decay is approached, the rate of change of the ^{210}Pb$_{ex}$ inventory decreases and, correspondingly, the resolution of the surface age determination derived from the total ^{210}Pb$_{ex}$ inventory degrades. In practice, resolving surface ages beyond 4 to 5 half-lives is difficult.

If the uniform atmospheric deposition rate D is constant, then the trend toward increased ^{10}Pb$_{ex}$ inventories with greater distance from the edge of a migrating channel can be used to determine the migration rate of the channel by recognizing that the rate of change of the activity N of a fallout radionuclide in surficial sediment due to atmospheric deposition and radioactive decay can be quantified as

$$\frac{\partial N(t)}{\partial t}=D-\lambda N(t). \tag{1}$$

The total inventory $N(t)$ at any time t is thus

$$N(t)=\int_0^t (D-\lambda N)dt. \tag{2}$$

Surface age $t_{surface}$ at a particular distance x from the channel edge can be expressed in terms of a constant and uniform migration rate M, namely,

$$t_{surface}=\frac{x}{M}. \tag{3}$$

Using this relationship, the total surface inventory can be written as

$$N(x)=\int_0^{x/M}(D-\lambda N)dx. \tag{4}$$

The initial condition is defined by the inherited ^{210}Pb$_{ex}$ inventory N_o

$$N(t=0,x=0)=N_o. \tag{5}$$

Integrating Eq. (4) subject to the initial condition (Eq. (5)), the total radionuclide inventory at any distance x from the edge of the channel is

$$N(x)=\frac{D}{\lambda}\left[1-\left(1-\frac{N_o\lambda}{D}\right)\exp^{\frac{-\lambda x}{M}}\right]. \tag{6}$$

Below we explore the applicability of this result.

3. Site descriptions

Transects of ^{210}Pb$_{ex}$ inventories were collected at three field sites selected based on the availability of sufficient historical aerial photography and orthoimagery to permit lateral channel migration rates to be determined by image analysis. The three field sites, one each in the Winooski and Connecticut Rivers in northern Vermont and one in the Genesee River in western New York (Fig. 1), all have watersheds with the same dominant surficial geology of glacial till

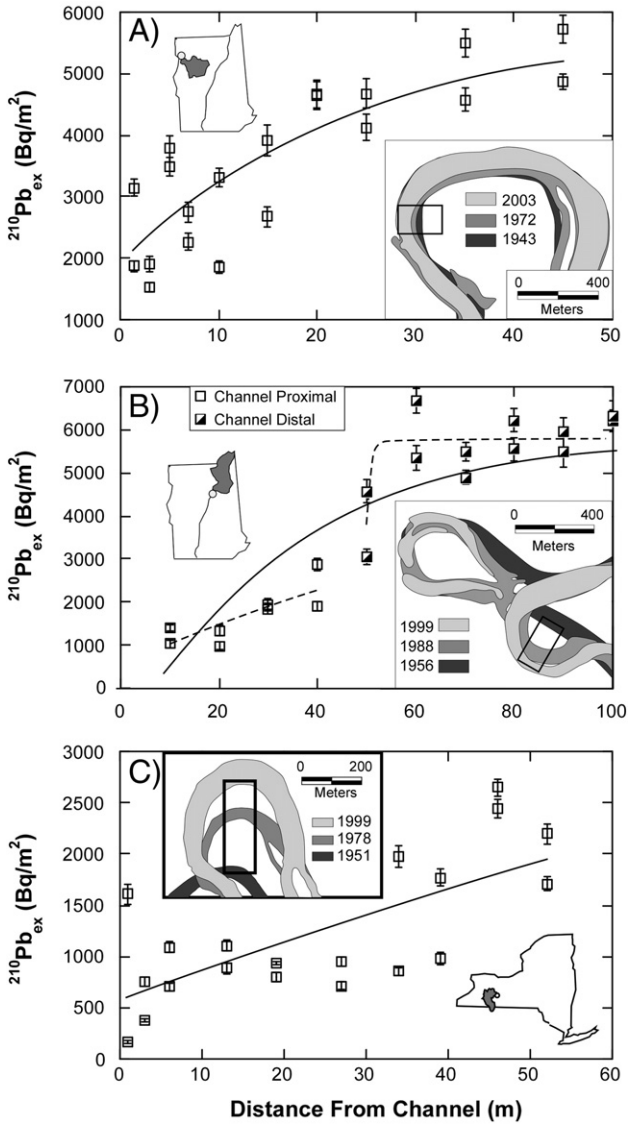

Fig. 1. Total ^{210}Pb$_{ex}$ inventory with distance from channel edge for the (A) Winooski, (B) Connecticut and (C) Genesee rivers. Solid curves are best fits to Eq. (6). Dashed curves are fits to Eq. (6) for channel proximal inventories and Eq. (7) for channel distal inventories. Error bars represent sample specific analytical error. Insets show watershed locations and historical channel locations with transect locations indicated by rectangular boxes.

with local alluvium and lacustrine deposits. All three sites are located in similar climatic regimes of the northeastern United States with precipitation more or less uniformly distributed throughout the year, thus decreasing variability between sites from meteoric differences in ^{210}Pb fallout. The sampled migrating river meander bends on each river have visual surface features, such as scroll bars, indicative of recent migration and the dominance of lateral over vertical migration (Melton, 1936; Nanson and Croke, 1992). Further, no historical agricultural use within the last 50 years is apparent at any of the migrating bends. Complete descriptions of each site follow.

3.1. Winooski River

The Winooski River (Fig. 1A) flows NW from central Vermont to the sampling site (44.537672N. 73.273762W.) located 1 km upstream of the mouth of the river on Lake Champlain near Burlington, VT. The watershed area upstream of the sampling site is ~2770 km^2. The channel width around the migrating bend averages ~100 m. Flow in the river has been regulated since 1917 by the Essex Junction hydroelectric dam located 270 km upstream and additionally, since 1992, by the Winooski One dam hydroelectric facility ~10 km upstream of the sampling site. Neither dam maintains a significant reservoir suggesting that mean annual flows have remained relatively constant over time. The mean annual discharge observed near the Winooski One dam is 51 m^3/s. The mean annual precipitation is ~85 cm. Near the sampling site, the active channel mean grain size ranges from fine to coarse sand. Average channel slope is 1.4×10^{-3} and average channel sinuosity is 2.2 from the mouth of the Winooski to 25 km upstream. Mean channel migration (calculated at 100 m intervals from the change in location of the inner bank on successive aerial photographs) of the reach extending 10 km upstream from the sampling site is 0.7 m/y.

3.2. Connecticut River

The Connecticut River (Fig. 1B) flows south from its headwaters in northern New Hampshire. The sampling site (44.625176N. 71.551323W.) on the Connecticut River is located upstream of Stratford, NH where the watershed area is 4295 km^2. The average channel width around the migrating bend is ~40–50 m. The sampling site lies in the longest (105 km) free-flowing reach of the Connecticut River. The Lyman Falls dam once stood 15 km upstream of the sampling site but was breached and removed in 1963. Standing 9 m high, the lower (Canaan) dam is located ~30 km upstream and has a reservoir of 2.5×10^5 m^3. Four other active, mainstem dams lie upstream of the lower dam on the Connecticut River. Flow at the sampling site is unaffected by the nearest downstream dam on the mainstem, Wilder dam. The mean annual discharge, observed 15 km upstream of the site, is 46 m^3/s and the mean annual precipitation is ~94 cm. Near the sampling site, active channel mean grain size ranges from fine sand to very fine gravel. Average channel slope is 9.5×10^{-5}, and average channel sinuosity is 2.1, measured $\pm$10.5 km from the sampling site. Mean channel migration (calculated at 100 m intervals from the change in location of the inner bank on successive aerial photographs) of the reach $\pm$10.5 km from the sampling site is 1.1 m/y.

3.3. Genesee River

The Genesee River (Fig. 1C) flows north from its headwaters in northwestern Pennsylvania to the sampled location (42.75558N. 77.85264W.) near Mount Morris in central New York State. The watershed area upstream of the sampling site on the Genesee River is 3600 km^2. The migrating bend at the sampling site is located 7 km downstream from the Mount Morris dam with no significant tributary inputs existing between the dam and sampling site. The 55-m-tall Mount Morris was built in 1951 as a low trap, flood control structure providing a reservoir storage volume of ~0.37 km^3. The average channel width around the migrating bend is ~65 m. The mean annual discharge over the years 1960–2007, measured at the gage 3.5 km downstream from the migrating bend, is 52 m^3/s. Mean annual precipitation in the region is ~84 cm/y. Near the sampling site, the active channel mean grain size ranges from fine to very coarse sand. Average channel slope is 7.7×10^{-4} and average channel sinuosity is 2.5 from Mount Morris dam to 26-km downstream. Mean channel migration (calculated at 100 m intervals from the change in location of the inner bank on successive aerial photographs) of the 26 km reach downstream of the dam is 0.8 m/y. The outer edge of the sampled migrating bed impinges upon a road that was relocated around the migrating bend.

4. Methods

Georectified historical topographic maps (USGS, 2010), aerial photographs, and orthophotographs (USDA, 2008) of the three sampling sites were used to reconstruct the channel geometries over the last 50–100 years. Regions visible in each image were classified as being either river channel or floodplain using an isodata unsupervised classification scheme. Migration rates were then determined by measuring the distance the inner (convex) channel bank has moved along a direction orthogonal to the channel over the time between successive photographs. Owing to rapid lateral migration rates at all three sites, errors in locating the channel edge because of image resolution and differences in discharge across different images are small relative to, say, the distance a channel migrates in a year or two.

Excess ^{210}Pb from atmospheric deposition in soils in the northeastern United States is generally limited to the upper 20 cm of the soil profile (Kaste et al., 2003). Accordingly, bulk core samples from the upper 20 cm of floodplain sediments were collected along transects starting from the convex channel edge of the migrating river bend. Transects were located within regions of the greatest migration as determined from the image analysis (Fig. 1). All transects were orientated perpendicular to the modern channel. At each site, floodplain bulk core samples were complemented by grab samples of surficial channel bed sediments collected from a region of the active located 2–5 m from the inner bank.

Bulk core samples were collected by hammering into the ground a 30-cm-long, 2.5-cm I.D. plastic tube to a depth of 20 cm at regularly spaced intervals of 5–10 m along the transect. Two bulk cores located ~1 m apart were taken at each lateral distance from the channel edge to provide data on spatial variability of radionuclide inventories. The channel edge was determined by the break in slope on topographic profiles measured along the transect. Ten sets of bulk cores were taken along each transect.

After collection, all samples were dried at 75 °C for at least 24 h. Samples with visible organic matter >2 mm were ground using a stainless steel Wiley Mill. All samples were then sieved to <2 mm and the sieved fraction sealed in plastic bags. No inorganic or ground organic samples had significant fractions >2 mm.

All samples were tightly packed into uniform-sized plastic containers (105 mL) with masses ranging from 80 to 190 g. To measure ^{210}Pb, ^{137}Cs, ^{226}Ra, and ^{7}Be activity, Canberra Intrinsic High Purity Germanium Detectors (HPGe) were used to quantify gamma ray emissions from the samples. Two organic litter samples were counted using a Canberra Germanium Well Detector because of a sample mass <5 g. Total ^{210}Pb activity was determined from gamma ray emissions measured at 46 keV. ^{226}Ra activity was determined using the ^{214}Pb gamma ray emission at 352 keV after the sample had been sealed for 3 weeks. For samples sealed <19 days prior to analysis, we used the 186 keV ^{226}Ra photopeak and account for the ^{235}U interference by simultaneously measuring the ^{238}U photopeak at 63 keV. Excess ^{210}Pb$_{ex}$ activity was determined by subtracting ^{226}Ra activity from the total ^{210}Pb activity.

Detector efficiency was determined by spiking representative organic and mineralized samples with a certified uranium ore. In order to account for the low photon energy of the ^{210}Pb gamma emission, a self-attenuation correction was made for each sample by measuring gamma ray transmission through each sample from a ^{210}Pb point source on top of the sample. Because of the small volume used in the well detector, we assumed that no significant self-attenuation occurs relative to the matrix-matched standard.

The two primary sources of measurement error involved in measuring the activity of ^{210}Pb via gamma spectroscopy are the uncertainty inherent in photon emission statistics and in background subtraction. The uncertainty inherent in photon emission statistics is directly related to the total number of decays or counts (n) recorded by the detector, where $\sigma_n = \sqrt{n}$. All samples were run until they accumulated between 750 and 1250 ^{210}Pb counts. The uncertainty from background subtraction was determined using the uncertainty of a linear fit of the spectral data surrounding the photopeak.

5. Results

5.1. Lateral migration rates

Average migration rates of laterally migrating bends determined using image analysis range from 1 to 5 m/y (Table 1). Over the entire 70-year time frame covered by the six different historical maps and images of the Winooski River (Fig. 1A inset), the migration rate of the Winooski River has been nearly constant at 1 m/y. In contrast, episodic events and nonconstant migration are apparent for the Connecticut River; differences in the channel geometry between the 1956 and 1988 images are consistent with an avulsion occurring just upstream between 1956 and 1988 (Fig. 1B inset). Therefore, the average migration rate from 1956 to 1999 (3.3 m/y) reflects both channel abandonment and "true" lateral migration post avulsion. The recent migration rate (1988–1999), which is dominated by lateral migration rather than channel abandonment, is closer to ca. 4.1 m/y (Table 1). Similarly, the outer bend of the Genesee River impinged upon a road beginning sometime between 1978 and 1994. Local residents indicate that further migration of the river was initially restrained until the road washed out. Now the road has been diverted around the migrating bend. Thus, the actual migration rate may have diverged from the long-term average over the last decade, initially slowing and then increasing rapidly.

Bulk core samples along transects across all three migrating bends show generally increasing ^{210}Pb$_{ex}$ inventories with distance from the channel (Fig. 1). Relative to the other sites, sediments from the Winooski River (whose deposition creates the floodplain surfaces and thus set N_o) have the highest ^{210}Pb$_{ex}$ activity (Table 1) and its floodplain has the highest and most variable inherited ^{210}Pb$_{ex}$ near channel inventories (Fig. 1A). In the more distal floodplain region, inventories increase more smoothly and become more spatially uniform as the variable inherited ^{210}Pb$_{ex}$ decays, overbank deposition becomes less likely (see below), and the more spatially uniform process of atmospheric deposition becomes the dominant control on ^{210}Pb$_{ex}$ inventories.

The Connecticut River has the least active channel sediment (Table 1) and, correspondingly, also the lowest inherited ^{210}Pb$_{ex}$ inventories. More distal floodplain inventories indicate two event histories separated by an abrupt inventory increase between 40 and 60 m along the transect (Fig. 1B). The abrupt inventory increase is likely due to the channel avulsion between 1956 and 1988.

The Genesee River ^{210}Pb$_{ex}$ inventories initially increase with distance from the channel, then plateau for a distance of about 20 m before sharply increasing again at a distance of 30–40 m from the channel edge (Fig. 1C). The trend observed at the other sites toward more uniformly increasing inventories in the channel distal samples as atmospheric deposition becomes the dominant control on ^{210}Pb$_{ex}$ inventories is less apparent at this site because of the moderately high inheritance (associated with moderate channel sediment activity) coupled with the relatively short transect length (~50 m) relative to the rapid average migration rate (ca. 5 m/y, Table 1).

Multiparameter optimization (Press et al., 1992) was used to determine the least squares best fits of Eq. (6) to the transect data. Best fits are shown by the solid lines in Fig. 1, and associated best fit estimates for the average migration rate M and initial ^{210}Pb$_{ex}$ inventory N_o are compared to the migration rates determined via the image analyses in Table 1.

To account for the two-stage migration history apparent at the Connecticut River site, a best fit of Eq. (6) to the channel proximal data was first used to determine the modern migration rate M_1 and N_o. If N_o is assumed constant over the entire transect history, then the channel distal inventories should follow

$$N(x) = \frac{D}{\lambda}\left[1-\left(1-\frac{N_o\lambda}{D}\right)exp^{\frac{-\lambda(x')}{M_2}}\right] \quad (7)$$

where M_2 is the average migration rate predicted by the variation in distal ^{210}Pb$_{ex}$ inventories and $x' = x - x_o$ where x_o is the location along the transect at which the inventory would equal N_o if the channel had continued to migrate at rate M_2. The best fits using this dual migration rate approach are shown by the dashed curves in Fig. 1B and yield a migration rate of $M_1 = 3.1 \pm 0.95$ m/y for the channel proximal region, similar to the ca. 4 m/y migration rate predicted from the historical images between 1988 and 1999 (Table 1). The predicted migration rate for the channel distal ^{210}Pb$_{ex}$ inventories is close to zero ($M_2 = 0.02$ m/y), again consistent with the idea that when the channel avulsed it simply cut a new channel close to the 1988 historical location and never migrated across this region of the transect.

Table 1
Migration rates and ^{210}Pb $_{ex}$ inheritance inventories.

Site	Image analysis		210 Pbex	
	M(m/y)	Best fit[a] M (m/y)[b]	N_o (Bq/m^2)	Channel ^{210} Pb$_{ex}$ (Bq/kg)[c]
Winooski	1.0	0.7 (0.2)	1881 (357)	14.1 ± 0.99
Connecticut				0.73 ± 0.97
Proximal	4.1	3.1 (0.95)	535 (397)	
Distal	Avulsion	0.02 (5100)	–	
Genesee	5.0	5.3 (1.4)	628 (212)	4.24 ± 0.3

[a] Best fit of Eq. (6) to inventories using D = 180 Bq/m^2/y(Kaste et al., 2003).
[b] Parentheses indicate twice standard deviation in best fit value.
[c] Mean ± standard deviation.

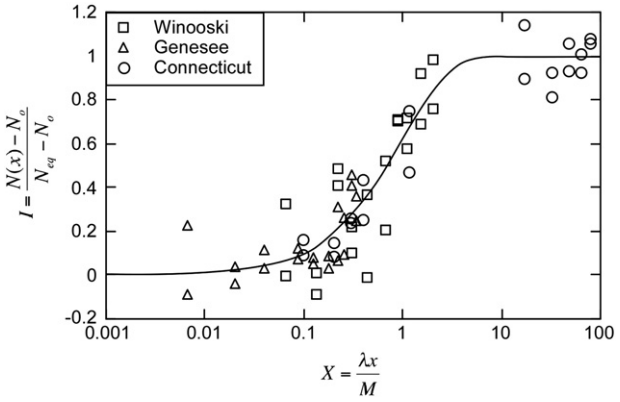

Fig. 2. Dimensionless time versus inventory for all sites. Solid curve shows variation in inventories predicted by Eq. (11).

To compare the three sites directly, in Fig. 2 dimensionless $^{210}Pb_{ex}$ inventories (I) are plotted as a function of dimensionless distance (X), where

$$I = \frac{N(x) - N_o}{N_{eq} - N_o}, \tag{8}$$

$$X = \frac{\lambda x}{M}, \tag{9}$$

$$N_{eq} = \frac{D}{\lambda}. \tag{10}$$

Substituting Eqs. (8)–(10) into Eq. (6) yields

$$I = 1 - exp(-X). \tag{11}$$

For the distal channel inventories from the Connecticut River, the dimensionless distance (X) becomes

$$X' = \frac{\lambda(x - x_o)}{M_2}. \tag{12}$$

The variation in inventories predicted by Eq. (11) is shown by the solid line in Fig. 2. Overall the fit to the model is good, suggesting the broad applicability of the $^{210}Pb_{ex}$ inventory methodology.

5.2. Sensitivity to vertical accretion

The results presented so far assume no vertical accretion due to, for example, overbank flood deposits. Because of the measureable isotopic activity of the channel sediment (Table 1), overbank flood deposits would increase the $^{210}Pb_{ex}$ inventory above that expected from inheritance and atmospheric deposition alone, leading to, if unaccounted for, an underestimation of the lateral migration rate. Accordingly, below we explore the sensitivity of our estimated lateral migration rates to vertical accretion.

In the presence of vertical accretion due to overbank flood deposits, the total surface inventory (Eq. (4)) can be rewritten as

$$N(x) = \int_0^{x/M} \left(D - \lambda N + \delta n_s \rho_s e^{-x/x_o}\right) dx \tag{13}$$

where δ is the vertical accretion rate, n the isotopic activity of the overbank sediment having a bulk density ρ_s, and x_o is the characteristic distance over which overbank deposition occurs. We assume vertical accretion caused by overbank deposition decreases exponentially with increasing distance from the channel edge (Pizzuto, 1987); Knox, 1972 #1304; Magilligan, 1992 #1305; Simm, 1998 #1306]. Integrating Eq. (13) subject to the initial condition (Eq. (5)), the total radionuclide inventory at any distance x from the edge of the channel is

$$N(x) = \frac{D}{\lambda}\left[1 - \left(1 - \frac{N_o\lambda}{D}\right) exp^{\frac{-\lambda x}{M}} + \frac{\delta n_s \rho_s}{D\left(1 - {}^{M}/_{\lambda x_o}\right)}\left(exp^{\frac{-x}{x_o}} - exp^{\frac{-\lambda x}{M}}\right)\right]. \tag{14}$$

To apply this model to our $^{210}Pb_{ex}$ inventory data, we approximate the initial activity of overbank sediment n_s as equal to the measured activity of channel sediment (Table 1), assume a typical sediment density of 2 g/cm^3, and estimate x_o from a least squares best fit of the topographic profile along each transect to a function of the form

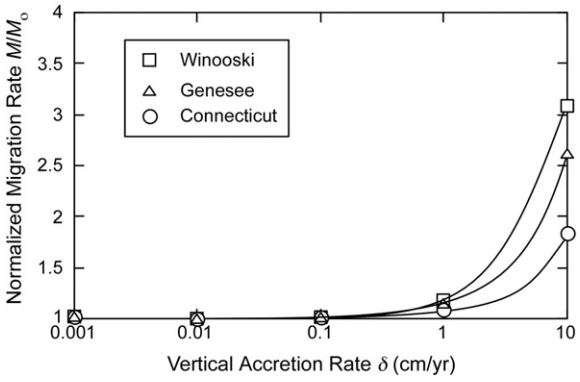

Fig 3. Lateral migration rate for all sites as a function of the vertical accretion rate as determined from best fits of inventory data to Eq. (14). Migration rates are normalized by the migration rate estimated in the absence of vertical accretion (Eq. (6)). For the Connecticut River, only the channel proximal data were used in the fitting.

$z(x) \propto 1 - exp^{-x/x_o}$. The migration rates from best fits to Eq. (14) as a function of vertical accretion rates are shown in Fig. 3. Here the migration rates are normalized by the best fit migration rates when there is no vertical accretion (Table 1).

Vertical accretion rates at our sites are unknown, but measured floodplain vertical accretion rates are typically of order 10^{-1}–10^{0} cm/y (Pizzuto, 1987; Rostan et al., 1997; Humphries et al., 2010; Wallinga et al., 2010). Vertical accretion rates at our sites are likely similar to those measured just to the north (0.1–1.1 cm/y) along rivers in southern Québec (Saint-Laurent et al., 2010). Fig. 3 demonstrates that for vertical accretion rates <~1 cm/y, the estimated lateral migration rates reported earlier are likely to underestimate true values by at most 10 to 20%. We conclude that in actively migrating systems, the assessment of lateral migration rates using the analysis advanced here is largely independent of vertical accretion in all but the most rapidly accreting systems, unsurprisingly, and thus certainly so in the settings considered here.

6. Conclusions

While each of the sites considered here has its own unique migration history, including both constant and episodic migration, each can be quantified using the same universal model (Eq. (11)), indicating that our approach provides a broadly applicable framework for quantifying channel migration where lateral accretion dominates. Our approach could be applied to other fallout radionuclides with shorter or longer half-lives that would be more appropriate for, respectively, rapid events (10^{-1} years) or historical scroll bar deposits (10^2–10^3 years). The broad spatial and temporal applicability of this method gives it the potential to succeed in quantifying fluvial migration rates and understanding floodplain histories where other methods have fallen short or have not been utilized because of spatial and environmental variability. Knowledge of migration rates derived from fallout radionuclides provides insight into the timeframes of sediment sequestration and delivery that impact a broad suite of geochemical and ecological processes. With the increased recent attention to the processes and timeframes of sourcing sediment from loci of erosion to its ultimate oceanic deposition ("sources-to-sink"), there has been progressive attention to understanding the timeframes of sediment sequestration and residence time (Phillips et al., 2007), the mass balance of sediment storage relative to sediment discharge (Lauer and Parker, 2008a; Lauer and Parker, 2008b), and the rates and spatial patterns of overbank deposition (Lecce, 1997; Magilligan et al., 1998; Aalto et al., 2008; Swanson et al., 2008). Results from this study contribute broadly to these recent research initiatives by revealing the time transgressive nature of lateral migration processes over decadal timescales and further indicate the spatial and temporal variation of sediment accumulation across floodplains.

Acknowledgements

This work was partially supported by the U.S. National Science Foundation (BCS-0724348 and EAR-060533).

References

Aalto, R., Lauer, J.W., Dietrich, W.E., 2008. Spatial and temporal dynamics of sediment accumulation and exchange along Strickland River floodplains (Papua New Guinea) over decadal-to-centennial timescales. J. Geophys. Res. 113 (F01S04). doi:10.1029/2006JF000627.

Appleby, P.G., 2008. Three decades of dating recent sediments by fallout radionuclides: a review. Holocene 18 (1), 83–93.

Appleby, P.G., Oldfield, F., 1992. Application of 210-Pb to sedimentation studies. In: Invanovich, M., Harman, R.S. (Eds.), Uranium-Series Disequilibrium: Application to Earth, Marine, and Environmental Sciences. Clarendon Press, Oxford, UK, pp. 731–778.

Billen, G., Lancelot, C., Meybeck, M., 1991. N, P, and Si retention along the aquatic continuum from land to ocean. In: Mantoura, R.F.C., Martin, J.-M., Wollast, R. (Eds.), Ocean Margin Processes in Global Change. John Wiley and Sons, New York, pp. 19–44.

Clapp, E.M., Bierman, P.R., Schick, A.P., Lekach, J., Enzel, Y., Caffee, M., 2000. Sediment yield exceeds sediment production in arid region drainage basins. Geology 28 (11), 995–998.

Hooke, J.M., 2008. Temporal variations in fluvial processses on an active meandering river over a 20-year period. Geomorphology 100 (1–2), 3–13.

Humphries, M.S., Kindness, A., Ellery, W.N., Hughes, J.C., Benitez-Nelson, C.R., 2010. 137Cs and 210Pb derived sediment accumulation rates and their role in the long-term development of the Mkuze River floodplain, South Africa. Geomorphology 119, 88–96.

Kaste, J.M., Friedland, A.J., Sturup, S., 2003. Using stable and radioactive isotopes to trace atmospherically deposited Pb in montane forest soils. Environ. Sci. Technol. 37 (16), 3560–3567.

Kaste, J.M., Heimsath, A.M., Hohmann, M., 2006. Quantifying sediment transport across an undisturbed prairie landscape using cesium-137 and high-resolution topography. Geomorphology 76, 430–440.

Lauer, J.W., Parker, G., 2008a. Modeling framework for sediment deposition, storage, and evacuation in the floodplain of a meandering river: application to the Clark Fork River, Montana. Water Resour. Res. 44, W08404. doi:10.1029/2006WR005529.

Lauer, J.W., Parker, G., 2008b. Net local removal of floodplain sediment by river meander migration. Geomorphology 96 (1–2), 123–149.

Lawler, D.M., 1993. The measurement of river bank erosion and lateral channel change: a review. Earth Surf. Process. Land. 18 (9), 777–821.

Lecce, S.A., 1997. Spatial patterns of historical overbank sedimentation and floodplain evolution: Blue River, Wisconsin. Geomorphology 18 (3–4), 265–277.

Magilligan, F.J., Phillips, J.D., James, L.A., Gomez, B., 1998. Geomorphic and sedimentological controls on the effectiveness of an extreme flood. J. Geol. 106 (1), 87–95.

Marcus, W.A., Meyer, G.A., Nimmo, D.R., 2001. Geomorphic control of persistent mine impacts in a Yellowstone Park stream and implications for the recovery of fluvial systems. Geology 29 (4), 355–358.

Melton, F.A., 1936. An empirical classification of flood-plain streams. Geogr. Rev. 28, 593–609.

Nanson, G.C., 1986. Episodes of vertical accretion and catastrophic stripping: a model of disequilibrium flood-plain development. Geol. Soc. Am. Bull. 97, 1467–1475.

Nanson, G.C., Croke, J.C., 1992. A genetic classification of floodplains. Geomorphology 4 (6), 459–486.

Nanson, G.C., Hickin, E.J., 1983. Channel migration and incision on the Beatton River. J. Hydraulic Eng. 109 (3), 327–337.

Papacostas, N.C., Bostick, B.C., Quicksall, A.N., Landis, J.D., Sampson, M., 2008. Geomorphic controls on groundwater arsenic distribution in the Mekong River Delta, Cambodia. Geology 36 (11), 891–894. doi:10.1130/g24791a.1.

Phillips, J.D., Marden, M., Gomez, B., 2007. Residence time of alluvium in an aggrading fluvial system. Earth Surface Processes And Landforms 32 (2), 307–316.

Pizzuto, J.E., 1987. Sediment diffusion during overbank flows. Sedimentology 34, 301–317.

Press, W.H., Teukolsky, S.A., Vetterling, W.T., Flannery, B.P., 1992. Numerical Recipes in C: The Art of Scientific Computing. Cambridge University Press, New York. 994.

Rostan, J.C., Juget, J., Brun, A.M., 1997. Sedimentation rates measurements in former channels of the upper Rhône river using Chernobyl 137Cs and 134Cs as tracers. Sci. Tot. Env 193, 251–262.

Saint-Laurent, D., Lavoie, L., Drouin, A., St-Laurent, J., Ghaleb, B., 2010. Floodplain sedimentation rates, soil properties and recent flood history in southern Québec. Global Planet. Change 70, 76–91.

Salant, N.L., Renshaw, C.E., Magilligan, F.J., Kaste, J.M., Nislow, K.H., Heimsath, A.M., 2007. The use of short-lived radionuclides to quantify transitional bed material transport in a regulated river. Earth Surface Processes And Landforms 32 (4), 509–524.

Svendsen, K.M., Renshaw, C.E., Magilligan, F.J., Nislow, K.H., Kaste, J.M., 2009. Flow and sediment regimes at tributary junctions on a regulated river: impact on sediment residence time and benthic macroinvertebrate communities. Hydrologoc Processes 23, 284–296.

Swanson, K.M., Watson, E., Aalto, R., Lauer, J.W., Bera, M.T., Marshall, A., Taylor, M.P., Apte, S.C., Dietrich, W.E., 2008. Sediment load and floodplain deposition rates: comparison of the Fly and Strickland rivers, Papua New Guinea. J. Geophys. Res. Earth Surf. 113. doi:10.1029/2006JF000623 F01S03.

USDA, 2008. Farm Service Agency Aerial Photography Field Office. United States Department of Agriculture, Salt Lake City, UT.

USGS, 2010. USGS Topographic Maps. United States Geological Survey, Reston, VA.

Wallbrink, P.J., Murray, A.S., 1996. Determining soil loss using the inventory ratio of excess lead-210 to cesium-137. Soil Sci. Soc. Am. J. 60 (4), 1201–1208.

Wallinga, J., Hobo, N., Cunningham, A.C., Versendaal, A.J., Makaske, B., Middlekoop, H., 2010. Sedimentation rates on embanked floodplains determined through quartz optical dating. Quat. Geochron. 5, 170–175.